

Flexible Carbon Nanotube–Cu₂O Hybrid Electrodes for Li-Ion Batteries

Anubha Goyal, Arava L. M. Reddy, and Pulickel M. Ajayan*

This study demonstrates the formation of a flexible and free-standing carbon nanotube–copper oxide–poly(vinylidene fluoride) (CNT–Cu₂O–PVDF) nanocomposite and its application as an electrode-separator material for Li-ion batteries. Binder-free hybrid electrodes are obtained by conformally coating CNTs with Cu₂O via electrodeposition and then embedding the resulting architecture into a porous poly(vinylidene fluoride–hexafluoropropylene) PVDF–HFP–SiO₂ polymer electrolyte membrane. The synergistic presence of high-capacity transition metal oxides and conductive CNTs results in twice the reversible areal capacity of 2.3 mAh cm⁻² as compared to 1.2 mAh cm⁻² for pure CNTs.

1. Introduction

Lithium-ion batteries command a major presence among all rechargeable battery systems, owing to their higher energy density and better efficiency and battery life as compared to alternatives.^[1] Improvements in Li-ion battery technology have been driven significantly by microelectronics that require lighter, thinner, and higher capacity batteries, particularly for portable devices.^[1–3] There is a particular interest in fabricating thin, flexible batteries with widespread applications in rolled-up displays, implantable devices, and smart cards.^[4,5] One of the major challenges in the development of these flexible batteries is to achieve a mechanically robust, lightweight system without compromising the electrochemical characteristics. This necessitates concerted improvements in the structural, electrochemical, and design aspects of the battery through innovations in constituent electrode, electrolyte, and separator materials.^[6,7]

Nanotechnology offers possible solutions in new material designs, with carbon nanotubes (CNTs) being an electrode material that holds great promise.^[8–10] The nanoscale 1D geometry and a collective set of exceptional mechanical,

electrical, and thermal properties, make CNTs highly favorable for energy-related applications in batteries, supercapacitors, and fuel cells.^[4,11–13] Aligned arrays of CNTs are particularly useful in flexible batteries as their 3D architecture offers both flexibility and mechanical robustness. They can also serve as physical supports for the integration of high-capacity materials such as transition metal oxides, since CNTs by themselves are limited by low capacity. In this regard, substantial efforts have been directed toward researching oxides of different transition metals such as nickel, iron, cobalt, and copper as possible electrode materials.^[14–17] These oxides have a high capacity as they operate based on the conversion reaction from metal to metal oxide, accompanied by the formation and decomposition of Li₂O, instead of the Li-ion intercalation/de-intercalation as in CNTs.^[18] Transitional metal oxides are attractive because of their low cost and high capacity, but they are plagued by issues related to slow cycling rates, poor capacity retention, and low electronic conductivity.^[19]

Integration of the two systems—CNTs and transition metal oxides—has proven effective in designing efficient electrodes.^[20–23] Though there are reports available on the successful dispersion of various metal oxides over randomly oriented carbon nanotubes, the deposition of transition metal oxides over aligned CNTs has remained a challenge. In the past, we have been successful in synthesizing MnO₂–CNT coaxial hybrid arrays for Li-ion batteries using a template approach.^[13] However, this technique is not feasible to obtain large-area electrodes. We have also shown the fabrication of

A. Goyal, A. L. M. Reddy, Prof. P. M. Ajayan
Department of Mechanical Engineering and Materials Science
Rice University
6100, Main Street Houston, Texas 77005, USA
E-mail: ajayan@rice.edu

DOI: 10.1002/sml.201002051

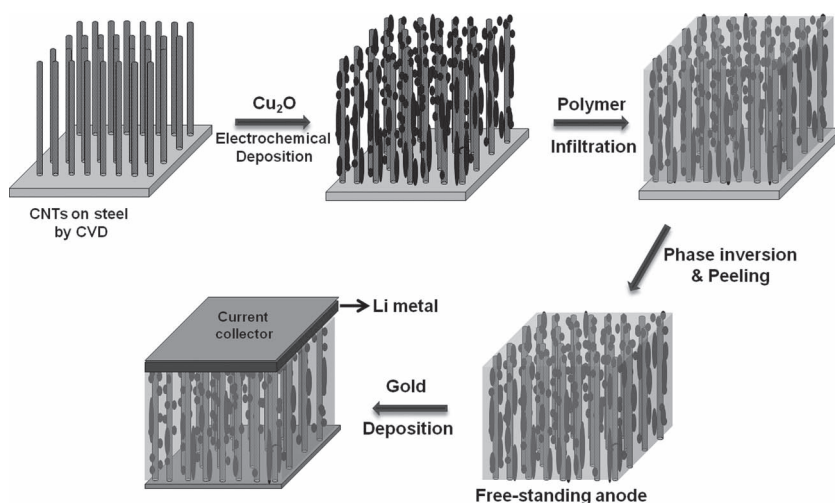


Figure 1. Fabrication schematic for Cu_2O -coated CNT electrodes. The CVD-grown CNTs were coated with copper oxide using electrodeposition. After polymer infiltration, the CNTs were peeled off the substrate to obtain free-standing electrodes on which a thin layer of gold was sputter-coated.

CNT–cellulose nanocomposite, which was flexible but demonstrated the relatively low capacity of 110 mAh g^{-1} .^[4] The present work is targeted towards addressing both the scalability problem associated with template approach and the poor electrochemical performance of the flexible composite. A flexible metal oxide–CNT composite has been developed that exhibits superior electrochemical behavior due to the incorporation of both the metal oxide and CNTs in a single system.

This study involves the fabrication of metal oxide-coated CNT electrodes fabricated via an electrodeposition technique, which is a simple and low-cost process for obtaining large-area electrodes. It synergistically combines the high capacity of Cu_2O and the 3D framework provided by the conductive CNTs to fabricate a novel, nanostructured, flexible electrode. The schematic in **Figure 1** delineates the synthesis procedure. Aligned CNTs were obtained on a steel substrate by a chemical vapor deposition (CVD) process and were then coated with Cu_2O using electrodeposition. The as-formed hybrid structure was embedded in a poly(vinylidene fluoride-hexafluoropropylene) (PVDF-HFP)- SiO_2 polymer electrolyte matrix in which porosity was introduced by phase inversion. PVDF-HFP is a widely chosen polymer electrolyte due to its good electrochemical and mechanical stability and

high ionic conductivity.^[24] Nanosized inorganic inclusions can enhance the mechanical strength and ionic conductivity of the polymer membrane besides improving its cycling ability and interfacial lithium stability.^[25] The membrane was made porous to increase its uptake of the liquid electrolyte and consequently enhance ionic conductivity.^[26] The composite film was peeled from the substrate to obtain the free-standing, flexible electrode.

2. Results and Discussion

Figures 2A,B are the scanning electron microscope (SEM) images of CNTs after the electrodeposition of copper oxide. From **Figure 2A**, it can be seen that the alignment of CNTs was evidently maintained post-electrodeposition. The high-magnification image reveals the

formation of a uniform and almost continuous conformal coating of copper oxide on the CNTs. The SEM and transmission electron microscope (TEM) images of pristine CNTs prior to electrodeposition are given in the Supporting Information (SI), **Figure S1** and **S2** respectively. The as-grown multiwalled CNTs are well aligned with a length of up to $300 \mu\text{m}$. The high-magnification image of CNTs shows ample free volume present in between the CNTs. The energy dispersive spectroscopy (EDS) spectrum obtained from the coated CNTs clearly indicates the presence of copper on them (SI, **Figure S3**).

Crystallinity of the coating was determined using X-ray diffractometry (XRD). The peaks in the XRD pattern (**Figure 3A**) of copper oxide-coated CNTs at 29.5° , 36.7° , 42.5° , 61.5° , and 73.4° correspond to $\{110\}$, $\{111\}$, $\{200\}$, $\{220\}$, and $\{311\}$ Bragg reflections from the cubic cuprite phase (Joint Committee on Powder Diffraction Standards #005–0667), thereby confirming the formation of crystalline Cu_2O on the CNTs. The other high-intensity peaks in the pattern at 44° , 50.9° , and 74.7° originate from the steel substrate and match

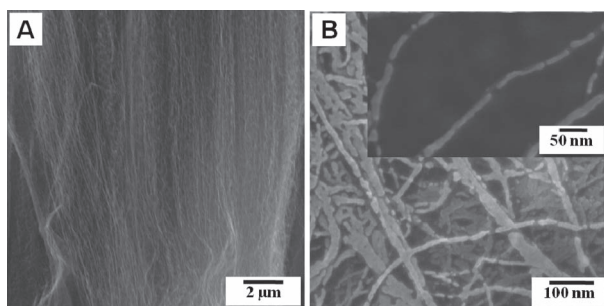


Figure 2. A,B) SEM images of copper oxide-coated CNTs. The inset shows a good conformal coverage of copper oxide on CNTs.

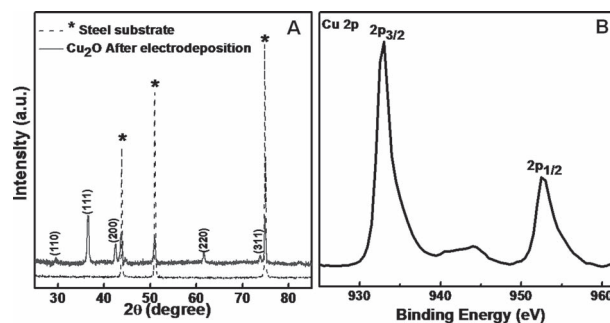


Figure 3. A) XRD pattern obtained from Cu_2O –CNT hybrids showing the crystalline nature of the Cu_2O coating. Peaks at 2θ values of 44° , 50.9° , and 74.7° originate from the steel substrate used for CNT growth. B) XPS spectrum of Cu_2O –CNT hybrid. The peak positions establish the presence of copper as Cu_2O .

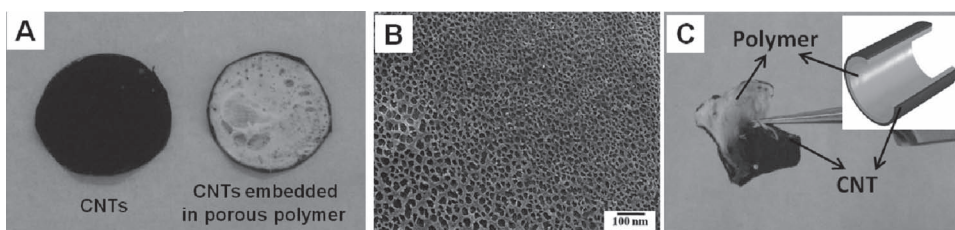
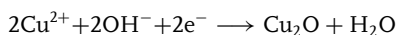
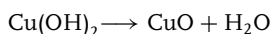


Figure 4. A) Photographs of pure CNTs and CNTs after polymer infiltration. B) SEM images revealing the porous nature of the PVDF-HFP-SiO₂ film after phase inversion. C) The photograph emphasizes the good flexibility of the peeled films.

with the control pattern obtained from a pure steel substrate. Cu₂O is also the expected phase in accordance with the well-established reaction mechanism.^[27] The electrodeposition proceeds through the formation of Cu(OH)₂ in the medium. The hydroxide decomposes to form CuO followed by its subsequent conversion to Cu₂O.



X-ray photoelectron spectroscopy studies were conducted to further confirm the oxidation state of copper and to verify the formation of Cu₂O. Figure 3B shows the Cu2p core-level spectrum recorded from the coated CNTs. The peak positions in the spectrum correspond to the binding energy of cuprous oxide. The spin-orbit coupling in copper results in two peaks centered at 933.1 and 953 eV from the 2p_{3/2} and 2p_{1/2} core levels.^[28] These XPS results, in conjunction with the XRD studies, firmly establish the formation of a pure Cu₂O coating on the CNTs and remove the possibility of CuO. This was further verified by Raman spectroscopy, which shows peaks corresponding to Cu₂O only (SI, Figure S4).^[29] After the detailed analysis of the as-formed coating, both pure and coated CNTs were embedded in the porous PVDF-HFP-SiO₂ membrane prepared by phase inversion. **Figure 4A** shows the photographs of the pristine, as-grown CNTs on the steel substrate with a very uniform growth all over the substrate and of the CNTs embedded in the porous polymer electrolyte membrane. Phase inversion results in a well-connected porous

membrane after solvent extraction, as seen in Figure 4B. The polymer film embedded with CNTs was peeled from the substrate. The film possesses very good flexibility, as evident from the photograph in Figure 4C. Due to their excellent flexibility, the membranes remain mechanically robust even on bending and thereby result in structurally strong, free-standing electrodes. The presence of the polymer film also makes an external separator redundant and contributes towards weight reduction of the electrode.

These free-standing electrodes were tested against Li metal for application in batteries. **Figure 5A,B** show the galvanostatic charge–discharge curves for the pure CNTs and the CNT–Cu₂O hybrid electrodes. The capacity for the first discharge is 2.3 mAh cm⁻² for the hybrid as compared to 1.2 mAh cm⁻² for pure CNTs. The decay in the capacity between the first and the second cycle is due to the formation of the solid electrolyte interphase layer on the electrodes.^[30] The capacity variation was recorded for a number of cycles: the comparison between the hybrid electrode and pure CNTs is shown in Figure 5C. The capacity subsequently saturates and, even after 15 cycles, the hybrid retains its good capacity and exhibits better performance. It gives a reversible specific capacity of 0.23 mAh cm⁻², in contrast to a significantly lower 0.11 mAh cm⁻² capacity achieved with pure CNTs. On a gravimetric basis, the hybrid and pure CNTs have a capacity of 305 and 115 mAh g⁻¹, respectively, after 15 cycles. This three times enhancement in capacity can be attributed to the dual mechanism in operation; the contributions from both the CNTs and Cu₂O. The highly conductive core of the CNTs gives a good electrical contact and a better conductivity,

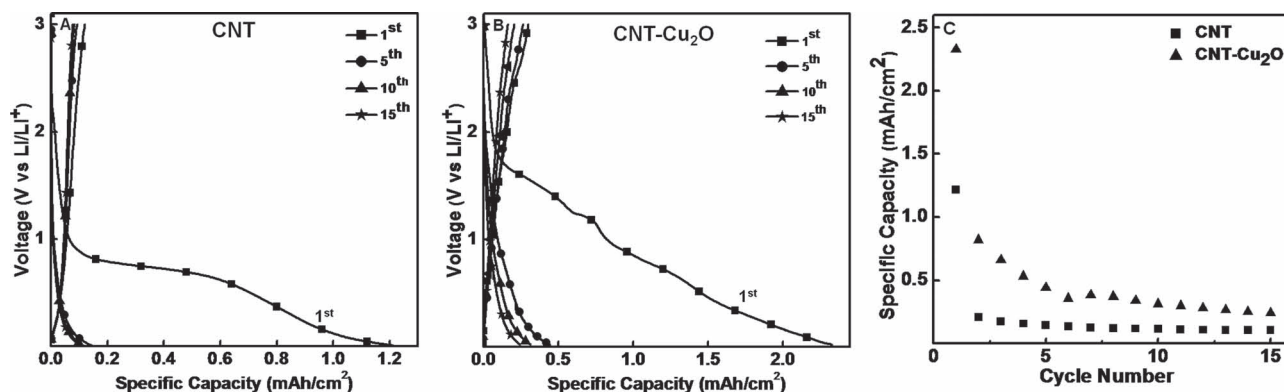
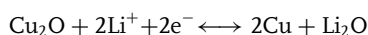


Figure 5. Charge–discharge voltage profiles of A) pure CNTs and B) CNT–Cu₂O hybrid between 0.02 and 3 V versus Li/Li⁺. C) Comparison of their electrochemical performance. The hybrid has a better capacity as compared to pure CNTs.

and their high aspect ratio helps to achieve the percolation threshold at much lower weights. Also, their aligned structure provides an easily accessible, regular, and porous path for the ions to diffuse and, unlike traditional carbon materials used as binderlike activated carbon, CNTs themselves behave as an active material. Although the good alignment assists in providing a high surface area for the Li-ion insertion/deinsertion in CNTs, they are limited by low capacity. The presence of copper oxide on the CNTs significantly improves their capacity by adding to the Li storage in the system. Unlike the classical Li-ion alloying and de-alloying mechanism present in CNTs, the reaction of Li-ion with copper oxide proceeds through Li insertion during the metal reduction, followed by its de-insertion during the oxidation process.^[18] This conversion reaction can be represented as:



The repeated Li-ion intercalation/deintercalation causes volume changes that can lead to material disintegration. This could significantly hamper battery performance through a loss in capacity and recyclability, but the presence of CNTs in the core of the hybrid system acts as a buffer to absorb these volume expansions.^[14] The CNT support, together with the polymer film, helps to maintain the structural integrity of the CNT–Cu₂O electrode even after repeated cycling.

3. Conclusion

A novel strategy has been developed for fabricating flexible high-capacity anodes for Li-ion batteries. Cu₂O was electrodeposited on aligned, CVD-grown CNTs, and the hybrid system was embedded in a porous PVDF-HFP–SiO₂ polymer matrix. This configuration obviates the need for a binder or external current collector, resulting in a highly desirable lightweight flexible geometry. CNTs provide a highly conductive physical framework for the deposition of high-capacity copper oxide. The introduction of copper oxide helps in mitigating the low capacity observed in pure CNTs and the hybrid shows an enhanced discharge capacity (2.3 mAh cm⁻²) in comparison to pure CNTs (1.2 mAh cm⁻²). This innovative methodology provides a new design and a better performing material, thereby opening avenues for advanced applications that require flexible electrodes. The design is particularly useful for applications requiring lightweight and miniaturized batteries.

4. Experimental Section

Synthesis: CNTs were grown by a chemical vapor deposition technique on a stainless steel substrate (Alfa Aesar Type 304), which was coated with predeposited catalyst; 10 nm aluminum followed by 1.5 nm iron using an e-beam evaporator.^[31] Aligned CNTs ≈300 μm were obtained through the decomposition of ethylene at 775 °C for 15 min in the presence of water vapor. An inert atmosphere was maintained throughout the growth period by a

constant flow of Ar/15%H₂ (1.3 slm (standard liters per minute)). The as grown CNTs were used for the cathodic electrodeposition of copper oxide using CuSO₄ solution (0.05 M) complexed with equimolar citric acid.^[27] The pH of the solution was maintained at 9 by using NaOH (1 M). The electrodeposition was carried out at room temperature in a conventional three-electrode setup consisting of a saturated Ag/AgCl reference electrode and a platinum counter-electrode. 40 deposition cycles were carried out at a potential of –1.05 V (standard calomel electrode, SCE) with a 4 s pulse width at an interval of 10 s between pulses. SI, Figure S5 shows a representative current-versus-time profile of the electrodeposition process. The CNTs were washed well with DI water after deposition and dried in a vacuum oven for a day.

After drying, the copper oxide-coated CNTs were embedded in a porous SiO₂–PVDF-HFP polymer electrolyte membrane prepared by a phase-inversion technique. To prepare the membranes, PVDF-HFP (Kynar 2801) and SiO₂ (Fumed Silica, CAB-O-SIL TS 530, Cabot Corporation) were dissolved in 4:1 weight ratio in a 10% by weight PVDF-HFP solution in acetone.^[25] Porous membranes were obtained by dipping the polymer composite with the embedded CNT–copper oxide in a water bath and drying it under vacuum for 24 h.^[32] The polymer membranes embedded with CNT–copper oxide were peeled from the substrate to obtain free-standing composite films that were characterized and then tested as an anode material after sputter-coating with 100 nm of gold for good electrical contact.

Characterization: Pristine CNTs were imaged using high-resolution transmission electron microscopy (JEOL 2100) at 200 kV. The phase and crystalline nature of electrodeposited copper oxide were determined using an XRD-Rigaku D/Max Ultima II operated at 40 kV. Morphological and elemental analyses were carried out using an SEM-FEI Quanta 400 operated at 20 kV. XPS measurements (XPS-PHI Quanterra SXM) were carried out using Al K_α radiation (1486.6 eV) incident at an angle of 45° to the sample. For electrochemical measurements, a Swagelok-type test cell was assembled in an argon-filled glove box, with CNT/PVDF-HFP as the working electrode/separator, lithium metal foil as the counter/reference electrode and 1 M LiPF₆ in 1:1 (v/v) solution of ethylene carbonate and dimethyl carbonate as the electrolyte. Galvanostatic charge–discharge testing was performed 45 μA cm⁻² within a voltage window of 0.02–3 V using a battery analyzer (Arbin Instruments BT2010).

Supporting Information

Supporting Information is available from the Wiley Online Library or from the author.

Acknowledgements

We acknowledge the financial support from National Science Foundation, Division of Materials Research Grant 06090077 and from the Army Research Office. The authors thank Dr. Robert Vajtai for the schematic of the flexible electrode in Figure 4C.

- [1] J. M. Tarascon, M. Armand, *Nature* **2001**, *414*, 359.
- [2] S. Megahed, B. Scrosati, *J. Power Sources* **1994**, *51*, 79.
- [3] W. A. V. Schalkwijk, B. Scrosati, *Advances in Lithium-Ion Batteries*, Kluwer Academic, NY, USA **2002**.
- [4] V. L. Pushparaj, M. M. Shaijumon, A. Kumar, S. Murugesan, L. Ci, R. Vajtai, R. J. Linhardt, O. Nalamasu, P. M. Ajayan, *Proc. Natl. Acad. Sci. USA* **2007**, *104*, 13574.
- [5] K. T. Nam, D. W. Kim, P. J. Yoo, C. Y. Chiang, N. Meethong, P. T. Hammond, Y. M. Chiang, A. M. Belcher, *Science* **2006**, *312*, 885.
- [6] B. Scrosati, *Nature* **1995**, *373*, 557.
- [7] M. Armand, J. M. Tarascon, *Nature* **2008**, *451*, 652.
- [8] H. Zhang, G. P. Cao, Y. S. Yang, *Energ. Environ. Sci.* **2009**, *2*, 932.
- [9] H. K. Liu, G. X. Wang, Z. P. Guo, J. Z. Wang, K. Konstantinov, *J. Nanosci. Nanotechnol.* **2006**, *6*, 1.
- [10] R. P. Raffaele, B. J. Landi, J. D. Harris, S. G. Bailey, A. F. Hepp, *Mater. Sci. Eng. B—Solid State Mater. Adv. Technol.* **2005**, *116*, 233.
- [11] B. J. Landi, M. J. Ganter, C. D. Cress, R. A. DiLeo, R. P. Raffaele, *Energ. Environ. Sci.* **2009**, *2*, 638.
- [12] W. Z. Li, X. Wang, Z. W. Chen, M. Waje, Y. S. Yan, *Langmuir* **2005**, *21*, 9386.
- [13] G. Centi, S. Perathoner, *Catal. Today* **2010**, *150*, 151.
- [14] X. H. Huang, J. P. Tu, X. H. Xia, X. L. Wang, J. Y. Xiang, L. Zhang, Y. Zhou, *J. Power Sources* **2009**, *188*, 588.
- [15] C. Q. Zhang, J. P. Tu, X. H. Huang, Y. F. Yuan, X. T. Chen, F. Mao, *J. Alloy. Compd.* **2007**, *441*, 52.
- [16] Y. Nuli, R. Zeng, P. Zhang, Z. P. Guo, H. K. Liu, *J. Power Sources* **2008**, *184*, 456.
- [17] W. Y. Li, L. N. Xu, J. Chen, *Adv. Funct. Mater.* **2005**, *15*, 851.
- [18] S. Grugeon, S. Laruelle, R. Herrera-Urbina, L. Dupont, P. Poizot, J. M. Tarascon, *J. Electrochem. Soc.* **2001**, *148*, A285.
- [19] J. Desilvestro, O. Haas, *J. Electrochem. Soc.* **1990**, *137*, C5.
- [20] S. Venkatachalam, H. W. Zhu, C. Masarapu, K. H. Hung, Z. Liu, K. Suenaga, B. Q. Wei, *ACS Nano* **2009**, *3*, 2177.
- [21] W. Dong, J. Sakamoto, B. Dunn, *J. Sol-Gel Sci. Technol.* **2003**, *26*, 641.
- [22] S. F. Zheng, J. S. Hu, L. S. Zhong, W. G. Song, L. J. Wan, Y. G. Guo, *Chem. Mater.* **2008**, *20*, 3617.
- [23] P. C. Chen, G. Z. Shen, Y. Shi, H. T. Chen, C. W. Zhou, *ACS Nano* **2010**, *4*, 4403.
- [24] J. Y. Song, Y. Y. Wang, C. C. Wan, *J. Electrochem. Soc.* **2000**, *147*, 3219.
- [25] X. M. He, Q. Shi, X. Zhou, C. R. Wan, C. Y. Jiang, *Electrochim. Acta* **2005**, *51*, 1069.
- [26] A. Subramania, N. T. K. Sundaram, A. R. S. Priya, G. V. Kumar, *J. Membr. Sci.* **2007**, *294*, 8.
- [27] V. D. Patake, S. S. Joshi, C. D. Lokhande, O. S. Joo, *Mater. Chem. Phys.* **2009**, *114*, 6.
- [28] T. Nagaura, K. Tozawa, *Progress in Batteries and Solar Cells*, JEC Press, OH, USA **1990**.
- [29] Y. S. Gong, C. P. Lee, C. K. Yang, *J. Appl. Phys.* **1995**, *77*, 5422.
- [30] K. Edstrom, T. Gustafsson, J. O. Thomas, *Electrochim. Acta* **2004**, *50*, 397.
- [31] L. J. Ci, S. M. Manikoth, X. S. Li, R. Vajtai, P. M. Ajayan, *Adv. Mater.* **2007**, *19*, 3300.
- [32] K. M. Kim, N. G. Park, K. S. Ryu, S. H. Chang, *Electrochim. Acta* **2006**, *51*, 5636.

Received: November 15, 2010
Revised: February 22, 2011
Published online: May 16, 2011